Non-Markovian rock-paper-scissors games

Ohad Vilk [1,*] Mauro Mobilia [2,†] and Michael Assaf [1,‡]
[1]Racah Institute of Physics, The Hebrew University of Jerusalem, Jerusalem 91904, Israel
[2]Department of Applied Mathematics, School of Mathematics, University of Leeds, Leeds LS2 9JT, United Kingdom

(Received 22 September 2024; accepted 22 May 2025; published 20 June 2025)

Evidence is mounting that species interactions often involve long-term memory, with highly varying waiting times between successive events and long-range temporal correlations. Accounting for memory undermines the common Markovian assumption, and dramatically impacts key ingredients of population dynamics including birth, foraging, predation, and competition processes. Here we study a critical aspect of population dynamics, namely, non-Markovian multispecies competition. This is done in the realm of the zero-sum rock-paper-scissors (zRPS) model that is broadly used in the life sciences to metaphorically describe cyclic competition among three interacting species. We develop a general non-Markovian formalism for multispecies dynamics, allowing us to determine the regions of the parameter space where each species dominates. In particular, when the dynamics are Markovian, the waiting times are exponentially distributed and the fate of the zRPS model in large well-mixed populations is encoded in a remarkably simple condition, often referred to as the "law of the weakest" (LOW), stating that the species with the lowest growth rate is the most likely to prevail. We show that the survival behavior and LOW of the zRPS model are critically affected by nonexponential waiting times and, especially, by their coefficient of variation. Our findings provide key insight into the influence of long waiting times on non-Markovian evolutionary processes.

DOI: 10.1103/4mm1-943p

I. INTRODUCTION

Ecosystems consist of a large number of competing species, and it is of paramount importance to study the mechanisms affecting their probability of extinction and survival. It is well known that random birth and death events cause demographic fluctuations that can ultimately lead to species extinction or fixation—when one species takes over the entire population. As demographic fluctuations are strong in small communities and weak in large populations, various dynamics as well as survival and fixation scenarios appear in communities of different size and structure; see, e.g., Refs. [1–18]. For example, experiments on three-strain colicinogenic microbial communities have demonstrated that cyclic rock-paper-scissors-like competition led to intriguing behavior, with only the colicin-resistant strain surviving in large well-mixed populations, and to the long-time coexistence of all species on Petri dishes [3]. In this context, "rock-paper-scissors" games have received much attention and served as paradigmatic models for the dynamics of species in cyclic competition; see, e.g., [3,4,6–8,11,14–17,19–39].

The conditions favoring one species over other competing ones generally depend on numerous complex factors, e.g., the availability of nutrients or the presence of toxins in the ecosystems. However, the fixation and survival probabilities of the zero-sum rock-paper-scissors (zRPS) model, in which what one gains is exactly what the opponent loses, satisfy a remarkably simple relation in large well-mixed populations [1,2,40]: the species with lowest per-capita predation-reproduction rate (lowest payoff) is the most likely to survive and fixate the population. This *counterintuitive* result, often referred to as the "law of the weakest" (LOW) [2,40], becomes asymptotically a zero-one law in large populations, where the species with lowest payoff fixates the population and the others go extinct with a probability approaching 1 [1,2,40]. The LOW has been studied in various settings; see, e.g., Refs. [1,2,15,16,40], including in recent laboratory-controlled experiments. Notably, Ref. [17] studied cyclic competition of three strains of *Escherichia coli* and found that the "weakest strain" dominates the microbial community.

The LOW has been derived when the underlying stochastic dynamics are interpreted as a Markov process, with exponentially distributed waiting times (also referred to as interevent, holding, or residence times); see, e.g., [41]. In many situations, however, species interactions may involve time delays or different timescales, often yielding memory effects and hence the violation of the Markov assumption. In this case, the waiting-time distribution (WTD) is no longer exponential, and this can significantly affect the evolutionary dynamics, resulting, e.g., in correlations, amplified oscillations, or enhanced extinction probabilities [42–49]. In the context of animal behavior, optimal search strategies are often related to

*Contact author: ohad.vilk@mail.huji.ac.il
†Contact author: m.mobilia@leeds.ac.uk
‡Contact author: michael.assaf@mail.huji.ac.il

nonexponentially distributed interevent times [42–46,50–52]. It has notably been reported that environmental variability, affecting resource availability, can result in a heavy-tailed WTD, which in turn shapes the population dynamics; see, e.g., [43,44]. For instance, heavy-tailed WTDs characterizing *Caenorhabditis elegans* dynamics, have recently been shown to be associated with slow adaptation and to yield long-range correlations [48].

While nonexponential WTDs have been found to lead to strong stochastic oscillations and to enhance extinction in a two-species predator-prey model [49], to the best of our knowledge, the fixation/survival behavior of zRPS games with non-Markovian dynamics has not been studied. In particular, it is unknown how the fixation properties change when the reactions have nonexponential WTDs. In this work, we systematically analyze how different examples of WTDs alter the LOW in the paradigmatic zRPS model, and hence shed further light on the influence of WTDs on the evolution of non-Markovian processes in the presence of long-term memory.

A. Basic model

We consider a well-mixed population of constant size N consisting of individuals of three species: n_A, n_B, and n_C individuals of species A, B, and C, respectively, with $n_A + n_B + n_C = N$. The species are in cyclic competition: A outcompetes B, which dominates C, which in turn kills and replaces A, closing the cycle. That is, in this general zRPS model, sometimes referred to as cyclic Lotka-Volterra model [6,12,15,16,20,22], each species is the predator of another and the prey of the third species. Each predator-prey interaction consists of a "predation with reproduction" event, where the prey is killed and simultaneously replaced by an individual of the predating species. The dynamics can thus be represented by the reactions [see Eq. (B1)]:

$$\begin{aligned} A+B &\xrightarrow{k_A/N} A+A, \\ B+C &\xrightarrow{k_B/N} B+B, \\ C+A &\xrightarrow{k_C/N} C+C, \end{aligned} \tag{1}$$

where k_A, k_B, k_C are predator-prey interaction rates.

Under Markov dynamics, in the mean-field (MF) limit where $N \to \infty$ and demographic fluctuations are negligible, denoting by $a = n_A/N$, $b = n_B/N$, and $c = n_C/N$ the respective fractions of A, B, and C in the population, the zRPS dynamics obey the set of rate equations [21]

$$\dot{a} = a(k_A b - k_C c), \quad \dot{b} = b(k_B c - k_A a), \quad \dot{c} = c(k_C a - k_B b), \tag{2}$$

where, here and henceforth, the dot denotes the time derivative. Here the equilibrium points are the absorbing steady states $(a, b, c) = \{(1, 0, 0), (0, 1, 0), (0, 0, 1)\}$ and the coexistence stationary point

$$\mathbf{s}^* \equiv (a^*, b^*, c^*) = (k_A + k_B + k_C)^{-1}(k_B, k_C, k_A). \tag{3}$$

The absorbing steady states correspond to each species prevailing in turn and are all saddles (unstable), whereas $\mathbf{s}^*$ is a marginally stable *nonlinear center*. In fact, Eqs. (2) admit the nontrivial constant of motion [21]

$$\mathcal{R}(t) \equiv a^{k_B} b^{k_C} c^{k_A}. \tag{4}$$

With the conservation of $\mathcal{R}$, the oscillatory dynamics governed by (2) are characterized by neutrally stable closed orbits, set by $\mathcal{R}(t) = \mathcal{R}(0)$, surrounding $\mathbf{s}^*$ in the ternary phase space simplex; see Fig. 1(a) and Appendix A. One of the aspects of this study is to analyze the robustness of the dynamics predicted by (2) when memory effects modify the form of these rate equations; see below.

In finite populations, with $N < \infty$, the zRPS dynamics are generally modeled as a Markov process with absorbing states [6,8,41,53–55]. In the presence of demographic fluctuations, stemming from randomly occurring birth and death events (see Appendix B), $\mathcal{R}(t)$ is no longer conserved. Here the stochastic trajectories in the phase space follow the MF orbits for a transient and perform random walks between them, before hitting a boundary and then a corner of the ternary simplex (phase space); see Fig. 1(a). This results in the extinction of two species and fixation of the third [6,12,14,15]. The ensuing fixation/survival behavior depends crucially on the fluctuations in the number of individuals of each species that scales as $\sqrt{N}$ (their fraction scales as $1/\sqrt{N}$). In this

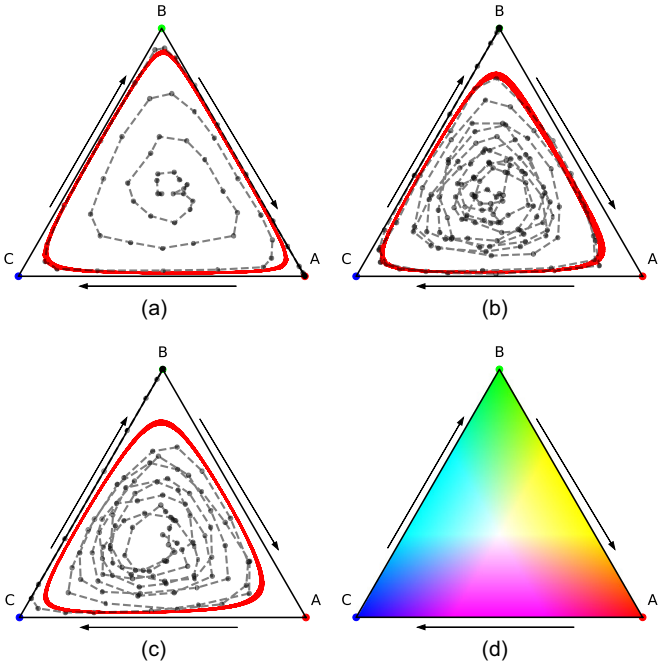

FIG. 1. (a)–(c) Dynamics in the the ternary simplex (phase space) for the zRPS model with exponential WTD in (a). In (b) and (c) the last two reactions of (1) have an exponential WTD, while the first reaction has a power-law WTD (8) with $(k_A, \alpha_A) = (0.8, 2.5)$ in (b), and a gamma WTD (16) with $(k_A, \alpha_A) = (0.8, 0.8)$ in (c). Furthermore, in (a)–(c) $k_B = k_C = 1$, and $N = 100$. Gray dotted lines: stochastic trajectories (single realization, clockwise dynamics) represent $(n_A, n_B, n_C)/N$, with initial conditions $(1/3, 1/3, 1/3)$. Red thick lines: deterministic outermost orbits; see Appendix C. Each corner corresponds to the fixation of the labeled species. (d) RGB diagram used to color code the fixation heatmaps, where the letters A (red), B (green), and C (blue) denote the winning species associated with each color; see text.

context, there has been a great interest in analyzing the influence of N on the species survival/fixation scenarios; see, e.g., Refs. [1,2,15–17,40]. A central question concerns the survival or, equivalently, fixation probability ϕ_i of species $i \in \{A, B, C\}$, defined as

$$\phi_i \equiv \lim_{t\to\infty} \text{Prob}\{n_i(t) = N | n_i(0)\} \approx \lim_{t\to\infty} \text{Prob}\{n_i(t) = N\}.$$

In large populations, $N \gg 1$, ϕ_i for the zRPS model with Markovian dynamics are independent of the initial conditions (except when initially one or more species are absent, or if the system starts very close to an absorbing boundary) [2,12,15,16,40] and satisfy the LOW. Thus, since throughout this paper we assume $N \gg 1$, without loss of generality, unless specified otherwise, we consider an equal initial number of individuals of each species, $n_i(0) = N/3$. We have also numerically confirmed that ϕ_A, ϕ_B, and ϕ_C are essentially independent of the initial condition when $N \gg 1$.

Throughout this paper, we focus on studying the influence of nonexponential WTD on ϕ_i in large populations, and deviations from the survival/fixation scenarios arising under Markovian dynamics that are briefly summarized below.

The mean time to extinction (MTE) t_{ext}, the average time for two species to go extinct (with fixation of the remaining one), is also a relevant quantity that depends on N. For the zRPS model with Markovian dynamics, the MTE has been shown to scale linearly with N [6,12,16]: $t_{\text{ext}} \sim N$. This is because extinction/fixation is reached after $O(N^2)$ reactions (random-walk steps in parameter space), each occurring on a timescale $O(1/N)$. For the zRPS model with nonexponential WTD, we still expect $t_{\text{ext}} \sim N$ whenever the underlying MF dynamics are characterized by closed orbits; see below and Figs. 1(b) and 1(c). Yet, a systematic study of the MTE for non-Markovian dynamics will be done elsewhere.

B. The law of the weakest under Markovian dynamics

As aforementioned, when reactions (1) have exponential WTDs (Markovian dynamics), the fixation probabilities of the zRPS games satisfy the LOW [1,2,12,15,16,40]: for sufficiently large N, typically $N \gtrsim 100$, the species $i \in \{A, B, C\}$ with the lowest rate $k_i \in \{k_A, k_B, k_C\}$ is the most likely to fixate the population [2,12,40]:

$$\phi_i > \phi_j \quad \text{if } k_i < k_j \text{ for } i \neq j \in \{A, B, C\}. \tag{5}$$

The LOW thus identifies the species i with the lowest k_i, dubbed the "weakest species," as the most likely to fixate/survive, with a probability $\phi_i \leqslant 1$ and $0 < \phi_j < \phi_i$, independent of the initial condition. Moreover, in very large populations the LOW becomes asymptotically a zero-one law [2,40]: it predicts that the weakest species has a probability one to survive while the others go extinct. Hence, for very large N, we have

$$\phi_m \to 1, \phi_n, \phi_l \to 0 \quad \text{if } k_m < k_n, k_l, \tag{6}$$

for (m, n, l) being all possible permutations of (A, B, C). If two species have the same interaction rate that is less than the other species' rate, the LOW predicts that the latter is most likely to go extinct, with a probability approaching one when $N \gg 1$, while the former have the same probability (approaching $1/2$ when $N \gg 1$) to fixate. The LOW thus predicts the regions of the parameter space in which each species is most likely to prevail [40]. For Markovian dynamics, according to Eqs. (5) and (6), the borders between these phases are given by simple linear relationships between the k_i's.

Insight into the LOW can be gained by considering the effect of demographic fluctuations on the closed orbits of the MF dynamics (2). When the stochastic trajectories in the phase space reach the outermost orbit defined by $\mathcal{R}(t) = 1/N$ [15,40], chance fluctuations cause the extinction of two species and fixation of the remaining one. From the coexistence equilibrium $\mathbf{s}^*$ and expression (4) of $\mathcal{R}$, it can be argued that the outermost orbit is closest to the edge leading to the fixation of the weakest species, yielding the LOW [40].

It is worth noting that a different scenario emerges in the Markovian zRPS model in small populations ($N \lesssim 20$): ϕ_i's satisfy the so-called "law of stay out" [40], where ϕ_A, ϕ_B, and ϕ_C depend on the initial condition [15,16,40,56]. Yet, here we consider large enough systems ($N \geqslant 10^2$) to disregard possible effects of the law of stay out.

C. RPS under exponential WTD

The LOW of the zRPS model has been amply studied under Markov dynamics. Here the rates k_i of reactions (1) are directly related to the mean of the *exponential* WTD, $\psi(\tau_i)$, between two reactions [41], where τ_i is the time between two successive events in which the predating species $i \in \{A, B, C\}$ kills and replaces a prey.

Generally, in a continuous-time Markov process, waiting times are distributed according to a one-parameter exponential function that can be written as

$$\psi_{\text{ex}}(\tau) = \lambda e^{-\lambda\tau}, \quad \langle\tau\rangle = \int_0^\infty \tau\psi_{\text{ex}}(\tau)d\tau = \lambda^{-1}, \tag{7}$$

with the single parameter λ coinciding with the inverse of $\langle\tau\rangle$, the mean time separating two successive events (reactions). In the zRPS model under Markov dynamics one has $\lambda_A = Nk_Aab$, $\lambda_B = Nk_Bbc$, and $\lambda_C = Nk_Cac$, for the reactions in Eq. (1). For $\psi_{\text{ex}}(\tau)$, the variance, coefficient of variation (CV, ratio of the standard deviation to the mean), and median are, respectively, $\text{var}(\tau) = \lambda^{-2}$, $\text{CV}(\tau) = 1$, and $\bar{\tau} = \ln 2/\lambda$.

Here we are interested in how the LOW is affected by WTDs that are *not* exponential, i.e., when the resulting zRPS dynamics are *non-Markovian* and include long-term memory. For simplicity our analytical derivation focuses on the case where the second and third reactions $B + C \to B + B$ and $C + A \to C + C$ are Markovian, with exponential WTDs, $\psi_i(\tau) = \lambda_i e^{-\lambda_i\tau}$ for $i = B, C$, whereas the first reaction $A + B \to A + A$ is non-Markovian and has a nonexponential WTD, denoted by $\psi_A(\tau)$. We consider two representative choices of a power-law and gamma WTDs [47] with a finite mean. The former allows us to study the influence of WTD with "heavy tails," commonly observed in ecology and biology [42,44–46,48,50–52], and the latter allows us to investigate the role of the WTD shape (skewness, median) on non-Markovian dynamics. Notably, we focus on the regime where the CV of the WTD is larger than that of an exponential, i.e., $\text{CV}(\tau) > 1$, where large deviations from the LOW are expected. The non-Markovian RPS processes considered in

this work are simulated following the method described in Appendix C.

II. RESULTS

A. RPS survival behavior with power-law WTD

Here we assume that the interevent time τ_A of the reaction $A+B \to A+A$ is distributed according to the two-parameter (Λ_A, α_A) power-law WTD:

$$\psi_A(\tau_A) = \Lambda_A \frac{\alpha_A}{(1+\Lambda_A \tau_A)^{\alpha_A+1}}, \quad \alpha_A > 1, \Lambda_A > 0, \tag{8}$$

whose mean, variance, and median are, respectively,

$$\langle \tau_A \rangle = \frac{1}{\Lambda_A(\alpha_A - 1)}, \quad \mathrm{var}(\tau_A) = \frac{\alpha_A \langle \tau_A \rangle^2}{(\alpha_A - 2)},$$
$$\bar{\tau}_A = \frac{2^{1/\alpha_A} - 1}{\Lambda_A}, \tag{9}$$

while $\mathrm{CV}_A \equiv \sqrt{\mathrm{var}(\tau_A)}/\langle \tau_A \rangle = \sqrt{\alpha_A/(\alpha_A - 2)}$. While the variance and CV_A are finite when $\alpha_A > 2$, one can still simulate the dynamics when $\alpha_A \leqslant 2$; see below.

The natural choice to directly compare the dynamics with a nonexponential WTD and its Markovian counterpart (with exponential WTDs) is to require the WTD's mean $\langle \tau_A \rangle$ to match the mean waiting time under Markovian dynamics λ_A^{-1} [57], where $\lambda_A = N k_A a b$. This yields

$$\Lambda_A = \lambda_A/(\alpha_A - 1). \tag{10}$$

Henceforth, we assume that (10) holds focusing on the $\alpha_A > 1$ regime (finite mean), and discuss our results chiefly in terms of the parameters k_A and α_A.

Notably, under Eq. (10), while the mean interevent time of the reaction $A+B \to A+A$ is the same as in the Markovian (exponential) case, the variance of τ_A with the power-law WTD is larger for any $\alpha_A > 1$ [for $1 < \alpha_A \leqslant 2$ the variance and CV_A of (8) diverge]; see Eq. (9). In fact, we notice that for the WTD (8), $\mathrm{CV}_A \to 1$ (as for an exponential WTD) as $\alpha_A \to \infty$, and $\mathrm{CV}_A \to \infty$ when $\alpha_A \to 2$. We thus expect the main differences from the exponentially distributed case to arise when $\alpha_A \gtrsim 1$, whereas we recover the LOW scenarios when $\alpha_A \to \infty$.

Importantly, as shown below, for a zRPS model with a heavy-tailed WTD the survival/fixation behavior is not fully captured by the LOW, as it cannot be solely inferred from the mean interevent times of the reactions (1). Intuitively, this stems from the fact that the mean time for a reaction to occur, related to the reaction rate, is not necessarily a good measure for typical events. In fact, while the mean time may be large, corresponding to a small reaction rate, the *typical* interevent times can actually be short; see Fig. 2 for an illustration with a gamma WTD [see Eq. (16)] for the reaction $A+B \to A+A$ (with the others being Markovian). In this case the *typical reaction rate* is larger than its mean and the LOW prediction does not generally capture the survival/fixation scenario: i.e., even if $k_A < k_B, k_C$, A may not be the most likely to survive. Notably, while this behavior can be expected for monotone-decreasing WTDs (e.g., power-law or gamma WTD with $\alpha \leqslant 1$; see below), it is not intuitively clear how the LOW changes for nonmonotone WTDs.

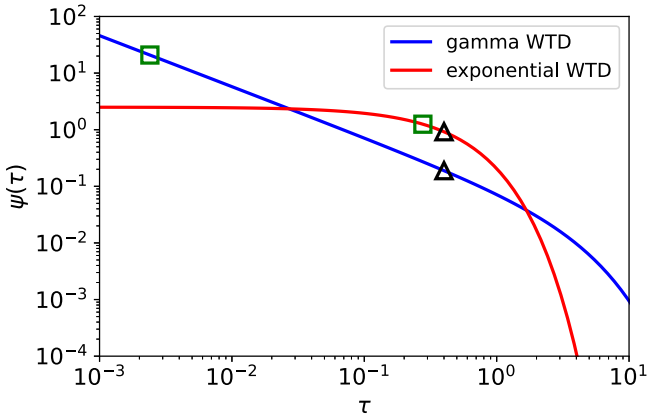

FIG. 2. An illustration of a gamma distribution (blue line) for $\alpha_A = 0.1$ and $\Lambda_A = 0.25$, such that the mean (black triangle) equals 0.4. The red line depicts an exponential distribution with the same mean. In contrast, the medians (green squares) differ significantly: 0.277 (exponential WTD) and 0.0024 (gamma WTD).

B. Generalized rate equations under power-law WTD

We now consider explicitly the case where the reaction $A+B \to A+A$ has an interevent time distribution, given by the power-law WTD (8), with the other two reactions of (1) having exponential WTDs. Analytical progress can be made using the formalism of continuous-time random walks [58,59], which leads to replace Eqs. (2) by the following generalized MF rate equations:

$$\begin{aligned} \dot{a} &= a\,b\,k_A \Theta(a,b,c) - a\,c\,k_C, \\ \dot{b} &= b\,c\,k_B - a\,b\,k_A \Theta(a,b,c), \\ \dot{c} &= a\,c\,k_C - b\,c\,k_B, \end{aligned} \tag{11}$$

where $\Theta(a,b,c) = \Theta_{\mathrm{PL}}(a,b,c)$ is the memory kernel in the power-law case (see Appendix B):

$$\Theta_{\mathrm{PL}}(a,b,c) = \chi\{[1 - e^{(\alpha_A-1)\chi}\alpha_A E_{\alpha_A+1}[(\alpha_A-1)\chi]]^{-1} - 1\}. \tag{12}$$

Here $\chi \equiv c(bk_B + ak_C)/(abk_A)$, $E_m(z) \equiv \int_1^\infty e^{-z\tau}\tau^{-m}d\tau$ is the exponential integral function, and we have set $\Lambda_A = \lambda_A/(\alpha - 1)$ with $\lambda_A = N k_A a b$. Thus, the mean interevent time of (8) equals that of an exponential WTD.

In fact, the generalized rate equations (11) can be used to find the coexistence equilibrium of the zRPS model with different nonexponential WTDs (see also the next section) and study the deviations that they cause to (3). When Eqs. (11) lead to closed orbits in the phase space, we can proceed as under Markovian dynamics, and infer from the location of the coexistence equilibrium and outermost orbit which species is the most likely to fixate/survive; see Figs. 1(b) and 1(c) and below.

While rate equations (11) with (12) cannot be solved analytically, a numerical solution for its coexistence stationary state (a^*, b^*, c^*), with λ_A given by Eq. (10), is shown in Figs. 3(a) and 3(b). Figure 3(a) shows (a^*, b^*, c^*) versus α_A, when $k_A = k_B = k_C = 1$ and the power-law WTD [Eq. (8)] has the same average $\langle \tau_A \rangle = 1/\lambda_A$ as under Markovian dynamics. As α_A increases, we recover the well-known Markovian result, with $a^* = b^* = c^* = 1/3$ for $\alpha_A \to \infty$ [see

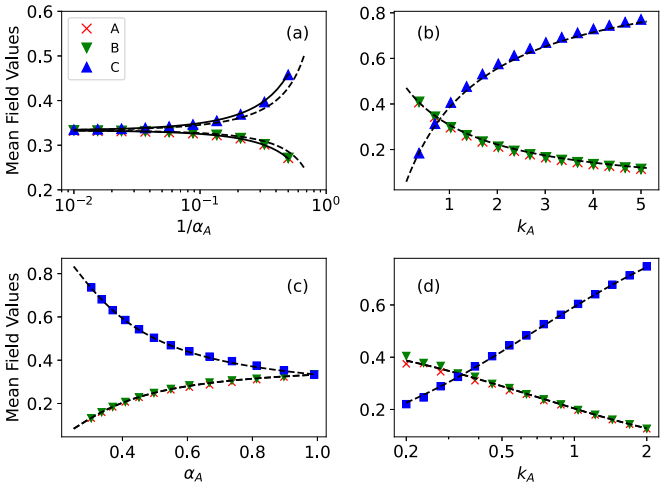

FIG. 3. Mean-field steady-state concentrations of A, B, and C versus α_A^{-1} and α_A (a, c) and k_A (b, d). In (a)–(b) and (c)–(d) the first reaction of (1) has a power-law and gamma WTD, respectively, while the second and third reactions have exponential WTDs. Markers are mean-field values (see legend) as obtained by averaging over stochastic simulations (see details in Appendix C). In all panels dashed lines show the analytical results: Eq. (14) in (a) and (b) and Eq. (20) in (c) and (d). The solid lines in (a) and (b) show the exact expression from numerically solving Eqs. (11) for $\dot{a} = \dot{b} = \dot{c} = 0$. Parameters are $k_A = k_B = k_C = 1$ (a), $\alpha_A = 3$ and $k_B = k_C = 1$ (b), $k_A = k_B = k_C = 1$ (c), and $\alpha_A = 0.4$ and $k_B = k_C = 1$ (d).

Eq. (3)], whereas $a^* = b^* < c^*$ when α_A is finite. Figure 3(b) shows the dependence of the coexistence state on k_A for fixed α_A.

The limit $\alpha_A \gg 1$ is particularly interesting as it is amenable to further analytical progress, and we aim at deriving the first subleading correction to (3) as a function of $\alpha_A^{-1} \ll 1$. To do so, we first approximate the exponential integral function $E_m(z)$ in the limit of $m, z \gg 1$, which yields $E_m(z) = \int_1^\infty e^{-z\ell}\ell^{-m}d\ell \simeq e^{-z}/(m+z)$ [60]. Using this approximation and the definition of χ [below Eq. (12)], in the limit of $\alpha_A \gg 1$ the memory kernel [Eq. (12)] becomes

$$\Theta_{\rm PL}(a, b, c) \simeq \alpha_A \chi[1 + (\alpha_A - 1)\chi]^{-1}, \tag{13}$$

where χ is a function of a, b, and c, given below Eq. (12). This result is formally valid for $\alpha_A \gg 1$, but remains rather accurate also for $\alpha_A \gtrsim 2$; see Figs. 3(a) and 3(b). As can be seen, at $\alpha_A \to \infty$ we recover the well-known form of $\Theta = 1$, such that the rate equations (2) of an exponential WTD are recovered, yielding the coexistence fixed point (3). However, at finite α_A, we find a nontrivial correction stemming from the power-law WTD of τ_A and non-Markovian nature of dynamics; see Figs. 3(a) and 3(b).

Focusing on $\alpha_A \gg 1$, here we analyze the interesting case where the predator-prey reaction rates obey the ratio $k_A : k_B : k_C = k : 1 : 1$, e.g., $k_B = k_C = 1, k_A = k$. (The coexistence equilibrium point for arbitrary k_A, k_B, and k_C is determined in in Appendix D.) Using Eq. (13), the coexistence equilibrium in this case reads

$$\{a^*, b^*, c^*\} = \frac{\{2(\alpha_A - 1), 2(\alpha_A - 1), k(2\alpha_A - 1)\}}{4(\alpha_A - 1) + k(2\alpha_A - 1)}. \tag{14}$$

This shows that a power-law WTD for τ_A generally changes the long-time zRPS dynamics. In particular, the tie predicted by Eq. (3) when $k = 1$ is broken (even at large α_A), with now $c^* = (1/3)\{1 - 2/[3(2\alpha_A - 1)]\}^{-1}$ and $a^* = b^* = (1/3)\{1+1/[6(\alpha_A - 1)]\}^{-1}$ at $\alpha_A \gg 1$, implying $c^* > a^*, b^*$ as found in Figs. 3(a) and 3(b). Notably, when α_A is not too close to 1, we have numerically verified that this coexistence equilibrium remains a nonlinear center, and species extinction/fixation thus occurs from its outermost orbit, according to the scenario outlined in the previous section; see also Appendix C. In Figs. 3(a) and 3(b) the numerical solution of the stationary (11) agrees well with the analytical approximation (14) for a^*, b^*, c^* and simulation results averaged over many stochastic realizations; see also Fig. 7 in Appendix C. In particular, Eq. (14) is quite accurate already when $\alpha_A \gtrsim 2$.

From Eq. (14) we can derive a useful expression for the critical value $k^* = k(\alpha_A)$ for which $a^*(k^*) = b^*(k^*) = c^*(k^*) = 1/3$. This can be found by demanding that $a^* = b^* = c^*$ in Eq. (14), which for $\alpha_A \gg 1$ yields

$$k^*(\alpha_A) \simeq 1 - (2\alpha_A - 1)^{-1}. \tag{15}$$

This critical value separates the $k - \alpha_A$ parameter space into two regions: $c^* > a^* = b^*$ where $k > k^*$ and $a^* = b^* > c^*$ where $k < k^*$. For sufficiently large α_A this informs on the location of the outermost orbit of (11) (see also Appendices A and C), implying that species A is the most likely to go extinct when $k > k^*$, while species A is the most likely to fixate the population when $k < k^*$. This is discussed below and remarkably demonstrated in Fig. 4.

C. RPS survival behavior with gamma WTD

We now consider a different non-Markovian scenario where the distribution of interevent times τ_A of $A + B \to A + A$ is a two-parameter (Λ_A, α_A) gamma distribution:

$$\psi_A(\tau_A) = \frac{\Lambda_A^{\alpha_A}}{\Gamma(\alpha_A)} \tau_A^{\alpha_A - 1} e^{-\Lambda_A \tau_A}, \quad \text{with} \quad \alpha_A, \Lambda_A > 0 \tag{16}$$

such that ψ_A is normalizable, with mean and variance

$$\langle \tau_A \rangle = \alpha_A/\Lambda_A, \quad \text{var}(\tau_A) = \alpha_A/\Lambda_A^2, \tag{17}$$

and $\text{CV}_A(\tau) = \alpha_A^{-1/2}$. The median does not admit a closed form but can be computed numerically for any (Λ_A, α_A). To directly compare the dynamics under gamma and exponential WTDs, we demand that the mean of the gamma WTD be $\langle \tau_A \rangle = 1/\lambda_A = 1/(Nk_A ab)$. This yields

$$\Lambda_A = \lambda_A \alpha_A. \tag{18}$$

For the gamma WTD, $\text{CV}_A \to 1$ when $\alpha_A \to 1$ whereas $\text{CV}_A \to 0$ when $\alpha_A \to \infty$, and $\text{CV}_A \to \infty$ when $\alpha_A \to 0$. We thus expect to essentially recover the LOW scenarios when $\alpha_A \to 1$, and to find strong deviations from it when $\alpha_A \to 0$. In the following, we focus on the regime of $\alpha_A \leqslant 1$ for which $\text{CV}_A \geqslant 1$. While the theory presented below is also applicable for $\alpha_A > 1$, a detailed treatment requires specific computational techniques that will be presented elsewhere (see Appendix C).

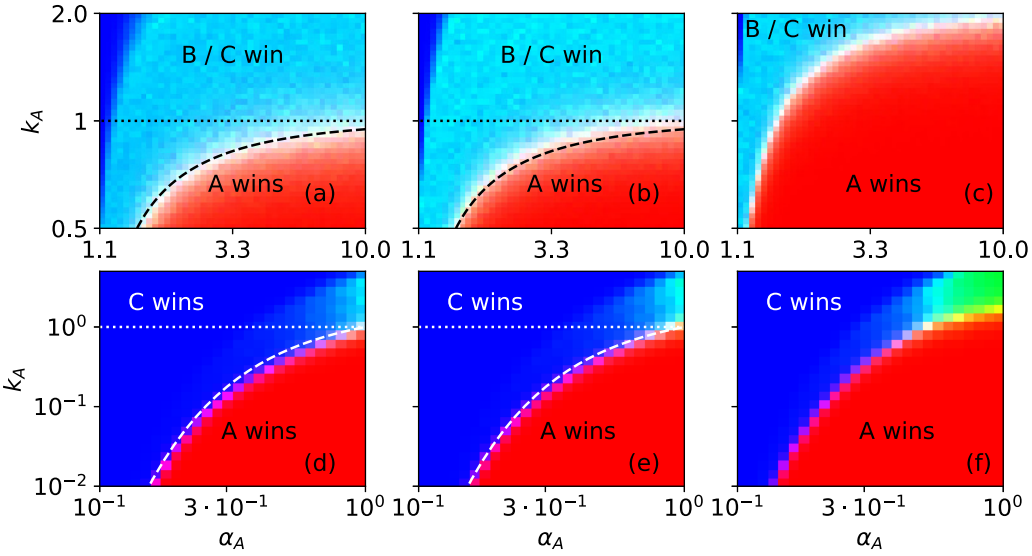

FIG. 4. RGB fixation heatmaps for power-law WTD (8) (a–c) and gamma WTD (16) (d–f) versus α_A and k_A, for $N = 999$ (a–c) and $N = 300$ (d–f) and $k_B = k_C = 1$. Red, green, and blue denote the fixation of A, B, and C, while cyan denotes the fixation of B and C with (approximately) equal probability; see diagram of Fig. 1(d). In (a) and (d) the WTDs for the second and third reactions of (1) are exponential. In (b) and (c) the second and third reactions of (1) have power-law WTDs with $\alpha_B = \alpha_C = 10$ (b) and $\alpha_B = \alpha_C = 1.5$ (c). In (e) and (f) the second and third reactions of (1) have gamma WTDs with $\alpha_B = \alpha_C = 0.9$ (e) and $\alpha_B = \alpha_C = 0.5$ (f). In (a)–(b) and (d)–(e) we compare our results to the theoretical curve for $k^*(\alpha)$ (dashed lines): Eq. (15) for (a) and (b) and Eq. (21) for (d) and (e); the dotted lines denote $k_A = 1$.

D. Generalized rate equations under gamma WTD

For a gamma WTD (16) of the first reaction of (1), proceeding as above, the generalized MF rate equations are given by (11), with the memory kernel (see Appendix B)

$$\Theta_G(a, b, c) = \chi[(1 + \chi/\alpha_A)^{\alpha_A} - 1]^{-1}, \tag{19}$$

where again $\chi \equiv c(bk_B + ak_C)/(abk_A)$, and we have assumed $\Lambda_A = \lambda_A\alpha_A$. When $\alpha_A = 1$, we recover $\Theta_G = 1$, yielding the MF Markovian dynamics.

Using memory kernel (19), we can solve for the steady state of Eqs. (11) exactly. Setting $\dot{a} = \dot{b} = \dot{c} = 0$ in (11), we find a relation for the coexistence equilibrium: $a^*b^*k_A\Theta_G(a^*, b^*, c^*) = k_Ca^*c^* = k_Bb^*c^*$. Here, for concreteness, we focus again on $k_A : k_B : k_C = k : 1 : 1$ (see Appendix D for the general case). Together with the relations $c^* = 1 - a^* - b^*$ and memory kernel (19), the coexistence equilibrium here becomes

$$\{a^*, b^*, c^*\} = \frac{\{2, 2, k\alpha_A(3^{1/\alpha_A} - 1)\}}{4 + k\alpha_A(3^{1/\alpha_A} - 1)}. \tag{20}$$

Thus, a^* and b^* are a decreasing function of k at fixed α_A. In addition, for $k = 1$, we have $a^* = b^* > 1/3$ and $c^* < 1/3$ when $\alpha_A > 1$, while $a^* = b^* < 1/3$ and $c^* > 1/3$ when $\alpha_A > 1$; see Figs. 3(c) and 3(d). At $\alpha_A \ll 1$, the fixed point becomes $a^* = b^* \approx (2/k\alpha_A)3^{-1/\alpha_A}$ and $c^* \approx 1 - (4/k\alpha_A)3^{-1/\alpha_A}$; i.e., a^* and b^* are exponentially small, while c^* approaches 1 exponentially.

A simple expression for the critical value $k^* = k(\alpha_A)$ for which $a^*(k^*) = b^*(k^*) = c^*(k^*) = 1/3$ is easily found by solving $\alpha_Ak^*(3^{1/\alpha_A} - 1) = 2$, yielding

$$k^*(\alpha_A) = 2[\alpha_A(3^{1/\alpha_A} - 1)]^{-1}. \tag{21}$$

This critical value separates the $k - \alpha_A$ parameter space into two regions, one in which $a^* = b^* > c^*$ (where $k < k^*$) and another in which $a^* = b^* < c^*$ (where $k > k^*$); see below.

E. Fixation heatmaps for the power-law WTD

A systematic way to visualize the influence of a heavy-tailed WTD on the zRPS fixation behavior is by means of fixation heatmaps shown in Fig. 4. These are RGB coded according to the diagram of Fig. 1(d) and report the triplet (ϕ_A, ϕ_B, ϕ_C) versus α_A and k_A, the mean rate (per A-B pair) of the first reaction of (1). According to Fig. 1(d), the phase dominated by species A, B, and C appears in red, green, and blue, respectively. In the color coding of Fig. 1(d), different levels of yellow, cyan, and magenta correspond, respectively, to a finite fixation probability of A and B, B and C, and C and A, while white encodes the same fixation probability for each species ($\phi_i \approx 1/3$).

In Fig. 4(a) we show results where the first reaction has power-law WTD (8) and the other reactions have exponential WTDs, with Λ_A given by (10), and $\lambda_A = Nk_Aab$, $\lambda_B = Nk_Bbc$ and $\lambda_C = Nk_Cac$. In Figs. 4(b) and 4(c) we report results obtained for the dynamics where all reactions are drawn from a power-law WTD, with $\alpha_B = \alpha_C = 10$ in (b), and $\alpha_B = \alpha_C = 1.5$ in (c). Here $\Lambda_B = \lambda_B/(\alpha_B - 1)$ and $\Lambda_C = \lambda_C/(\alpha_C - 1)$; see Eq. (10). As a reference, it is useful to consider the fixation heatmap predicted by the LOW for Markovian dynamics with exponential WTD: when $k_B = k_C = 1$, A dominates (red phase) for $k_A < 1$ and B and C dominate (cyan phase) for $k_A > 1$, separated by $k_A = 1$ (dotted lines in Fig. 4).

The heatmap diagram of Fig. 4(a) is mostly characterized by a red phase dominated by A ($\phi_A \approx 1$, $\phi_B \approx \phi_C \approx 0$), and

a cyan phase where B and C are the prevailing species ($\phi_A \approx 0, \phi_B \approx \phi_C \approx 1/2$). The border between these phases is an increasing function of α_A. When α_A approaches 1, the dynamics of (11) are not necessarily characterized by closed orbits, and a third phase, not predicted by the LOW, emerges in blue: it corresponds to the dominance of C ($\phi_A \approx \phi_B \approx 0, \phi_C \approx 1$), with breaking of the B/C symmetry. Here, as $\alpha_A \to 1$, the typical interevent time (median) becomes much smaller than the mean [see Eq. (9)]. As a result, the typical production rate of A individuals is very high at the expense of B individuals. Thus, the population of C can grow almost without opposition from its predator, species B, that is rapidly consumed by A, and hence C eventually fixates the entire population when $\alpha_A \approx 1$. Notably, Eqs. (11) support this analysis: as $\alpha_A \to 1$, memory kernel (12) becomes very large, $\Theta_{PL} \gg 1$, which yields $c^* \to 1$, and $a^*, b^* \to 0$. In contrast, when $\alpha_A \gg 1$, we recover the LOW predictions, and the separation between the red and cyan phases occurs around k^* (dashed line) given by (15). Remarkably, the prediction of k^* as a separating curve turns out to be valid also at $\alpha_A \gtrsim 1$. Here, as α_A approaches 1 and the median increasingly deviates from the mean, a striking departure from the LOW is observed; i.e., it is necessary to significantly lower k_A (much below 1) for A to win. The diagram of Fig. 4(b) is quantitatively similar to that of Fig. 4(a). This is because for large values of α_B, α_C, the power-law WTDs for the corresponding reactions are close to the exponential WTDs considered in Fig. 4(a).

The heatmap of Fig. 4(c) is characterized by the same phases as in Figs. 4(a) and 4(b), but with some major quantitative differences. In particular, we notice that the separation between the cyan and red phases in Fig. 4(c) occurs for values of k_A much higher than 1 (predicted by the LOW). This stems from the fact that the typical rates of the last two predator-prey reactions of (1) are higher than their corresponding means, giving rise to the fixation of A even for $k_A > 1$.

F. Fixation heatmaps for the gamma WTD

In Figs. 4(d)–4(f) we report the fixation heatmaps for the zRPS dynamics with gamma WTD for the reaction $A + B \to A + A$ as a function of k_A and α_A. Here, the WTD is given by (16) and the parameters (Λ_A, α) satisfy Eq. (18). In Fig. 4(d), the WTDs of the other two reactions are exponential. As expected, the survival/fixation behavior reproduces the LOW scenario at $\alpha_A = 1$: with an A-dominated (red) phase where $k_A < 1$ and a (cyan) phase dominated by B/C where $k_A > 1$. In Figs. 4(d) and 4(e) the white dotted line separates the two phases predicted by the LOW. This has to be contrasted with the critical value (21), shown as the dashed white curve, which separates the phases where A (red) dominates and where it does not dominate (blue/cyan region). In Figs. 4(d) and 4(e), the non-Markovian dynamics results in the fixation of A where $k_A(\alpha_A) < k_A^*(\alpha_A)$ which is the region of the phase space where $c^* < 1/3$; see Eq. (20). In this red region of the parameter space the coexistence equilibrium is thus closest to the A-B edge of Fig. 1, and species A is hence the most likely to fixate the population. The opposite occurs when $k_A(\alpha_A) > k_A^*(\alpha)$: species B or C prevail and A goes extinct. While the zRPS with gamma WTD reproduces the LOW predictions for α_A close to 1, with B and C most likely to prevail with the same probability where $k_A > 1$, the B/C symmetry is broken when α_A is distinctly below 1, and in this case C is the most likely to prevail as indicated by the blue phase in Figs. 4(d)–4(f).

Notably, the striking symmetry-breaking effect in the case of the gamma WTD is not predicted by the LOW and is not captured by the MF approximation. We note that a similar, but less striking, effect is also observed with power-law WTD in the narrow region where $\alpha_A \to 1$; see Figs. 4(a)–4(c). We conjecture that the stark contrast between the power-law and gamma WTD results stem from the ratio of the median to the mean of the WTD. Indeed, for the gamma WTD as α_A decreases below 1, the ratio between the median and mean goes to zero much more rapidly than in the power-law case (as α_A goes to 1); see, e.g., Fig. 2. Hence, the extreme scenario of almost complete depletion of B and takeover by C species occurs much earlier with the gamma WTD.

We notice that the nontrivial curve of $k_A = k^*$ given by (21) determines the separation between the phases where species A dominates (red) and where it loses (blue/cyan) with excellent accuracy. While for practical reasons, the numerical simulations are limited to $\alpha_A \leqslant 1$ (see Appendix C), we expect that the phases in which A is dominant and where it loses is determined by k^* also for $\alpha_A > 1$. In fact, when $\alpha_A > 1$, the gamma WTD is unimodal, with the mean and median being increasingly closer as α_A increases, and coinciding when $\alpha_A \to \infty$. Thus, when $\alpha_A > 1$, A can prevail also for $k_A > 1$, assuming that the fixation dynamics are qualitatively similar to those in the $\alpha_A \lesssim 1$ regime. In particular, at $\alpha_A \to \infty$, A prevails as long as $k_A < 2/\ln 3 \simeq 1.82$; see Eq. (20).

In Figs. 4(e) and 4(f), the last two reactions of (1) occur with interevent times that are also distributed according to a gamma WTD [Eq. (16)] with the equivalent of (18) for Λ_B and Λ_C. In Fig. 4(e) we take $\alpha_B = \alpha_C = 0.9$ and the resulting heatmap is very similar to that in Fig. 4(d). Yet in Fig. 4(f) $\alpha_B = \alpha_C = 0.5$ and the separating interface markedly changes. Even when $k_A = k_B = k_C = 1$, the values of α_B and α_C, hence the shape of the WTDs, change the range of k_A for which the LOW predictions are reproduced. In particular, when $\alpha_B = \alpha_C = 0.5$, species A dominates for higher values of k_A than under Markovian dynamics, and thus, the red region in Fig. 4(f) is larger than in Figs. 4(d) and 4(e) [see also Figs. 4(a)–4(c)]. We also notice that for $k_A \gg 1$ and $\alpha_A > \alpha_B, \alpha_C$ a green B-dominated phase appears in Fig. 4(f). Notably, both cases of symmetry breaking—dominance of C for $\alpha_A < \alpha_B, \alpha_C$, and B for $\alpha_A > \alpha_B, \alpha_C$—are not captured by MF theory. Thus, the observed symmetry breaking and dominance of either of the species may strongly depend on the full set of WTDs of all reactions rather than on a simple hierarchy.

G. Comparison of power-law and gamma WTDs

To further compare the effect of the power-law and gamma WTDs on the RPS survival scenarios, we plot in Fig. 5 the fixation maps under power-law and gamma WTDs versus the average waiting time $\langle \tau_A \rangle$ and coefficient of variation CV_A. This allows us to directly compare the effect of these different WTDs. As expected, in both panels for $CV_A = 1$ we fully reproduce the predictions of the LOW for exponential WTDs:

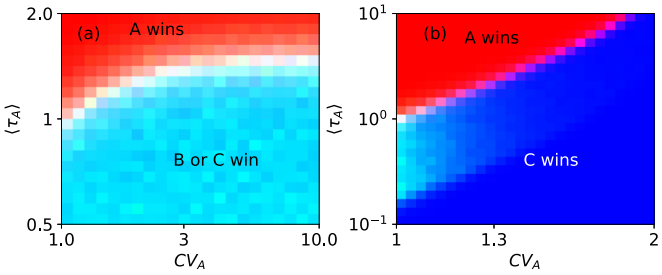

FIG. 5. RGB fixation heatmaps (based on the diagram of Fig. 1) for power-law (a) and gamma (b) WTDs of the first reaction of (1): mean interevent time $\langle\tau_A\rangle$ versus coefficient of variation CV_A. Here $N = 999$ and $k_B = k_C = 1$.

species A is the most likely to fixate the population (red phase) when $\langle\tau_A\rangle > 1$ ($k_A < 1$), whereas species B and C are the most likely to survive (same probability) and A goes extinct (cyan phase) when $\langle\tau_A\rangle < 1$ ($k_A > 1$). When $CV_A > 1$, the survival scenarios drastically deviate from the LOW predictions for the two cases considered here. When the first reaction has a power-law WTD, the white interface (equal fixation probability for all species) is a concave function which gradually changes as CV_A grows; see Fig. 5(a). Here, as CV_A is increased, larger $\langle\tau_A\rangle$ (smaller k_A) is required for A to win, with saturation of $\langle\tau_A\rangle$ when $CV_A \gg 1$. A much more pronounced effect is observed in the case of the gamma WTD with $\alpha_A \leqslant 1$ shown in Fig. 5(b). Here the white interface is a convex function and is much steeper than in the power-law case, with no observable saturation. Remarkably, when CV_A grows by a factor of 2, in order for A to still win, $\langle\tau_A\rangle$ (k_A) needs to increase (decrease) by a factor of >10; see Fig. 5(b). A similar increase in CV_A in the power-law case leads to an increase in $\langle\tau_A\rangle$ of only $\sim$40%; see Fig. 5(a).

Moreover, as also observed in Fig. 4, in the power-law case the white interface separates fixation of A (red regime) and extinction of A accompanied by equal fixation probability of B and C (cyan regime). In contrast, in the case of the gamma WTD with $\alpha_A \leqslant 1$, the interface separates fixation of A (red regime) and C (blue regime), and symmetry between B and C is broken; see Fig. 5. This is because for the gamma WTD, increasing CV_A has a much stronger effect on decreasing the typical interevent time than in the power-law case.

III. DISCUSSION

Evidence is mounting that waiting times between successive events play an important role in shaping evolutionary processes across biology and ecology. For instance, optimal foraging strategies have been linked to heavy-tailed waiting time distributions (WTDs) [42–46]. Moreover, with the development of microfluidic devices and single-cell experiments, the role of the reproduction time distribution on microbial growth has received significant attention [47,61,62]. Here we studied the influence of WTDs on the fate of the paradigmatic zero-sum rock-paper-scissors (zRPS) game between three species in cyclic competition, which is broadly used in biology and ecology [3,6–8,12,14–17,19–24,28,55,63,64]. The zRPS dynamics are classically modeled in terms of Markov processes, with exponential WTDs, and their final state satisfies the simple "law of the weakest" (LOW) [40] stating that the species that is most likely to fixate is the one with the lowest predation-reproduction (predator-prey) rate. Here we have shown that the LOW predictions are drastically altered in the non-Markovian zRPS model with nonexponential WTDs.

By combining analytical arguments and extensive stochastic simulations, we investigated the fixation probability of each species when at least one of the zRPS reactions has a nonexponential WTD, and we have focused on the two-parameter power-law and gamma WTDs. The former is related to anomalous diffusion [43], abundantly found in animal behavior, while the latter is often used to model the reproduction of microbial cells [47,61]. Keeping the same mean for all WTDs, we found that the fate of the zRPS dynamics is drastically affected by the features of the nonexponential WTD: the conditions under which one species is most likely to fixate depend nontrivially on the WTD parameters in addition to the reaction rates. We visualized our findings in fixation heatmap diagrams identifying the parameter regions dominated by each species. Depending on the WTD parameters, the phase in which one species dominates over the others can be enhanced or reduced with respect to the predictions of the LOW; see Figs. 4 and 5.

The major deviations from the LOW arise when the difference between the "typical" and "mean" interevent times (difference between the median and mean of the WTD) increases. By focusing on positively skewed distributions (like the exponential WTD), we showed that the region of dominance of the species whose reproduction is governed by the nonexponential WTD strongly depends on the WTD coefficient of variation (CV). The region of dominance of each species thus shrinks or grows with respect to the LOW predictions, depending on whether CV $>$ 1 or CV $<$ 1; e.g., in Fig. 5, the phase dominated by species A shrinks as CV $>$ 1. In addition, the symmetry between the other two species, a signature of exponential WTDs, is expected to be broken when the ratio between the median and mean vanishes. Our analytical arguments are based on the analysis of generalized MF rate equations. These involve memory kernels derived from the underlying non-Markovian master equations. While it would be desirable to establish a physical interpretation of the memory kernels, this is beyond the scope of this study. Yet, our work is readily applicable for a wide class of nonexponential WTDs, including scenarios in which species switch between multiple internal behavioral states, each having a distinct WTD, or empirical distributions which are directly inferred from data.

We believe that our analysis of the influence of nonexponential WTDs on the fate of the zRPS model can help shed further light on non-Markovian evolutionary dynamics and can help motivate further studies. Besides a physical derivation of the memory kernels, understanding how the mean fixation time of each species is affected by general nonexponential WTDs is an open question. Moreover, as a number of microbial experiments have been modeled using RPS dynamics [3,17], we expect that the effects of interevent time distributions on species in cyclic competition can be tested in laboratory-controlled experiments by employing our theoretical approach.

ACKNOWLEDGMENT

M.A. and O.V. acknowledge support from ISF Grant No. 531/20. M.M. thankfully acknowledges support of the EPSRC Grant No. EP/V014439/1.

DATA AVAILABILITY

Data and codes that support our work are available at [65].

APPENDIX A: STABILITY ANALYSIS IN THE NON-MARKOVIAN CASE

Here we briefly study the linear stability of the coexistence equilibrium (a^*, b^*, c^*) in the case of nonexponential WTD for the first reaction. As stated in the main text, with exponential WTDs, the MF rate equations (2) admit the constant of motion (4). In the phase space, the MF dynamics are therefore characterized by closed orbits surrounding (3) that is a (nonlinear) center; see Fig. 1(a). In fact, the Jacobian of (2) evaluated at (3) has two conjugate purely imaginary eigenvalues, denoted by $\{\beta i, -\beta i\}$ where β depends on the k_i values. In the case of $k_A = k_B = k_C = 1$, $\beta = -1/\sqrt{3}$.

Interestingly, when the first reaction of (1) has a power-law WTD and $\alpha_A \gg 1$, the Jacobian of (11) evaluated at (D1) also has a pair of conjugate purely imaginary eigenvalues of the form $\{(\beta + \beta_{PL}/\alpha_A)i, -(\beta + \beta_{PL}/\alpha_A)i\}$, where β_{PL} depends on k_i. In the case of $k_A = k_B = k_C = 1$, β is identical to the exponential case, and $\beta_{PL} = -1/(6\sqrt{3})$. Moreover, the quantity (4) is conserved by (11) to leading order in $1/\alpha_A$: $d\mathcal{R}/dt = \mathcal{R}(\Theta_{PL} - 1)k_A(k_B b - k_C a) = O(\mathcal{R}/\alpha_A)$, where we have used (13). This indicates that when $\alpha_A \gg 1$, the phase space dynamics prescribed by (11) are characterized by closed orbits surrounding the equilibrium (D1), where $k_B b^* - k_C a^* = 0$, for long transients; see Fig. 1(b). This behavior is qualitatively similar to that predicted by (2). However, the location of (a^*, b^*, c^*) and the shape of the orbits around it now depend on the nonexponential WTD parameter α_A, yielding deviations from the survival/fixation scenarios predicted by the LOW; see main text. While this analysis cannot be extended for arbitrary values of α_A, our extensive numerical simulations have confirmed that (a^*, b^*, c^*) is a nonlinear center for most values $\alpha_A > 1$; see Fig. 1(b).

A similar analysis can be done in the case of gamma WTD, when α_A is close to 1. Introducing $\epsilon = \alpha_A - 1$, for $|\epsilon| \ll 1$, the coexistence equilibrium (a^*, b^*, c^*), given by (D2), is again a center associated with two purely imaginary conjugate eigenvalues, $\{(\beta + \beta_G\epsilon)i, -(\beta + \beta_G\epsilon)i\}$. For $k_A = k_B = k_C = 1$, β is identical to the exponential case, and $\beta_G = (3\ln 3 - 2)/(6\sqrt{3})$. In fact, the quantity (4) is again conserved by the generalized rate equations (11) [with (19)] to leading order in ϵ when $\alpha \approx 1$: $d\mathcal{R}/dt = \mathcal{R}(\Theta_G - 1)k_A(k_B b - k_C a) = O(\mathcal{R}\epsilon)$, where we have used (D3). This again indicates that when $|\epsilon| \ll 1$, the phase space dynamics prescribed by (11) are characterized by closed orbits surrounding (D4); see Fig. 1(c). Thus, the survival scenario can again be inferred from the location of (a^*, b^*, c^*).

Notably, in the regime of $\alpha_A = O(1)$ in the power-law case, and $|\alpha_A - 1| = O(1)$ in the gamma case, we cannot prove in general that the dynamics include closed orbits. Nevertheless, our extensive numerical simulations show that, as long as α is not to close to 1 (in the power-law case) and to 0 (in the gamma case), closed orbits around the equilibrium state are still observed.

APPENDIX B: GENERALIZED RATE EQUATIONS

In this appendix, we outline the derivation of the generalized rate equations (11) with the memory kernel (12) in the case of a power-law WTD (8), and with the memory kernel (19) in the case of a gamma WTD (16). In the following, we respectively number the reactions $A + B \to A + B$, $B + C \to B + B$ and $C + A \to C + C$ as the first, second, and third reaction, and henceforth denote their WTDs by $\psi_A(\tau_A)$, $\psi_B(\tau_B)$, and $\psi_C(\tau_C)$.

We begin by writing the master equation for the probability $P_{n_A,n_B,n_C}(t)$ to find n_A, n_B, and n_C individuals of type A, B, and C, at time t. For Markovian dynamics, where all reactions have exponential WTDs, one obtains

$$\begin{aligned}\dot{P}_{\mathbf{n}}(t) = &\frac{k_A}{N}\left(E_{n_A,n_B}^{-1,+1} - 1\right)n_A n_B P_{\mathbf{n}}(t)\\ &+ \frac{k_B}{N}\left(E_{n_B,n_C}^{-1,+1} - 1\right)n_B n_C P_{\mathbf{n}}(t)\\ &+ \frac{k_C}{N}\left(E_{n_A,n_C}^{+1,-1} - 1\right)n_A n_C P_{\mathbf{n}}(t),\end{aligned} \tag{B1}$$

where $N = n_A + n_B + n_C$ is the total (constant) population size. Here we have defined a step operator for brevity of notation, $E_{k_1,k_2}^{j_1,j_2} f(k_1, k_2) = f(k_1 + j_1, k_2 + j_2)$, and denoted the population sizes by a vector $\mathbf{n} = \{n_A, n_B, n_C\}$. In the general case of reactions with nonexponential WTDs, the master equation becomes nonlocal in time; i.e., the current state depends on the entire history of the process with prescribed memory kernels that depend on the WTDs of the different processes; see below. In this case, Eq. (B1) becomes

$$\begin{aligned}\dot{P}_{\mathbf{n}}(t) = &k_A\left(E_{n_A,n_B}^{-1,+1} - 1\right)\int_0^t M_A(\mathbf{n}, t')P_{\mathbf{n}}(t - t')dt'\\ &+ k_B\left(E_{n_B,n_C}^{-1,+1} - 1\right)\int_0^t M_B(\mathbf{n}, t')P_{\mathbf{n}}(t - t')dt'\\ &+ k_C\left(E_{n_A,n_C}^{+1,-1} - 1\right)\int_0^t M_C(\mathbf{n}, t')P_{\mathbf{n}}(t - t')dt'.\end{aligned} \tag{B2}$$

Here $M_A(\mathbf{n}, t)$, $M_B(\mathbf{n}, t)$, and $M_C(\mathbf{n}, t)$ are the (yet to be found) memory kernels for the creation of A, B, and C, respectively, and the constant N was absorbed in these kernels. Following the derivation in [58,59,66] we find the memory kernels by Laplace transforming Eq. (B2). We first define the probability density for the first reaction to occur at time t while the other two reactions *do not* occur until t:

$$\Phi_A(t) = \psi_A(t)\int_t^\infty \psi_B(\tau)d\tau \int_t^\infty \psi_C(\tau)d\tau, \tag{B3}$$

where $\Phi_B(t)$ and $\Phi_C(t)$ are defined similarly. Note that, in addition to their time dependence, Φ_A, Φ_B, and Φ_C may also depend on n_A, n_B, and n_C. It can be shown that the memory kernels in Laplace space satisfy [58,59,66]

$$\tilde{M}_X(s) = s\tilde{\Phi}_X(s)[1 - \tilde{\Phi}_A(s) - \tilde{\Phi}_B(s) - \tilde{\Phi}_C(s)]^{-1}, \tag{B4}$$

where $X = \{A, B, C\}$, $\tilde{\Phi}_X$ denotes the Laplace transform of Eq. (B3), and s is the Laplace variable.

We now explicitly compute the memory kernels in the case of power-law WTD for the first reaction given by Eq. (8) with $\Lambda_A = \lambda_A/(\alpha_A - 1)$, and exponential WTDs for the second and third reactions, such that $\psi_B(\tau) = \lambda_B e^{-\lambda_B \tau}$ and $\psi_C(\tau) = \lambda_C e^{-\lambda_C \tau}$. Computing the Laplace transforms of Eq. (B3), $\tilde{\Phi}$, plugging the result into Eq. (B4), putting $\lambda_A = k_A n_A n_B/N$, $\lambda_B = k_B n_B n_C/N$ and $\lambda_C = k_C n_A n_C/N$, and taking the leading-order result with respect to $N \gg 1$, one obtains $\tilde{M}_B(s) = N k_B b\, c$ and $\tilde{M}_C(s) = N k_C a\, c$, where we have used the notation for the population fractions $a = n_A/N$, $b = n_B/N$ and $c = n_C/N$. In addition, we find $\tilde{M}_A(s) = N k_A a\, b\, \Theta_{PL}(a, b, c) + O(s)$, where $\Theta_{PL}(a, b, c)$ is given by Eq. (12). As all the memory kernels are constant in s in the leading order, performing an inverse Laplace-transform yields to leading order:

$$M_A(a, b, c, t) = N k_A a\, b\, \Theta_{PL}(a, b, c)\, \delta(t),$$
$$M_B(a, b, c, t) = N k_B b\, c\, \delta(t), \quad M_C(a, b, c, t) = N k_C a\, c\, \delta(t), \tag{B5}$$

where $\delta(t)$ is the Dirac delta function. Plugging these memory kernels into master equation (B2), all the integrals over time yield the integrands evaluated at time t, and one obtains

$$\begin{aligned}\dot{P}_{\mathbf{n}}(t) = {} & \frac{k_A}{N}\left(E^{-1,+1}_{n_A,n_B} - 1\right) n_A n_B \Theta_{PL}(\mathbf{n}) P_{\mathbf{n}}(t) \\ & + \frac{k_B}{N}\left(E^{-1,+1}_{n_B,n_C} - 1\right) n_B n_C P_{\mathbf{n}}(t) \\ & + \frac{k_C}{N}\left(E^{+1,-1}_{n_A,n_C} - 1\right) n_A n_C P_{\mathbf{n}}(t).\end{aligned} \tag{B6}$$

This equation coincides with master equation (B1) up to the factor of $\Theta_{PL}(\mathbf{n})$, which is the signature of the non-Markovian nature of the first reaction. As a result, and using the definition of the species averages

$$\bar{n}_A = \sum_{\mathbf{n}} n_A P_{\mathbf{n}}(t), \quad \bar{n}_B = \sum_{\mathbf{n}} n_B P_{\mathbf{n}}(t), \quad \bar{n}_C = \sum_{\mathbf{n}} n_C P_{\mathbf{n}}(t), \tag{B7}$$

in Eq. (B6), we arrive at rate equations (11) for $\bar{a} = \bar{n}_A/N$, $\bar{b} = \bar{n}_B/N$ and $\bar{c} = \bar{n}_C/N$, with $\Theta_{PL}(a, b, c)$ given by Eq. (12). Note that, in the MF limit, $N \to \infty$, the average species fractions $\bar{a}, \bar{b}, \bar{c}$ coincide with the fractions $a = n_A/N$, $b = n_B/N$, and $c = n_C/N$, and, for brevity, the latter have been used in all the MF equations in the main text [e.g., Eqs. (2) and (11)].

Similarly, the memory kernel and rate equations for the gamma WTD can be found via Eq. (16) for the first reaction with $\Lambda_A = \lambda_A \alpha_A$, and repeating the above steps.

APPENDIX C: COMPUTATIONAL METHODS

1. Simulations

Here we summarize the simulation methods we have used. We start with a description of the original Gillespie algorithm [67], followed by the Laplace Gillespie algorithm [68] used to simulate nonexponential WTD.

a. Gillespie algorithm

The original Gillespie algorithm assumes $\mathcal{N}$ independent Poisson processes with rates λ_i $(1 \leqslant i \leqslant \mathcal{N})$ running in parallel. The combined effect of these Poisson processes results in a superposed Poisson process with a total rate $\sum_{i=1}^{\mathcal{N}} \lambda_i$. The algorithm steps are as follows:

(1) *Time increment (Δt) calculation*. The time to the next event in the superposed Poisson process follows the exponential distribution:

$$\varphi(\Delta t) = \left(\sum_{i=1}^{N} \lambda_i\right) e^{-(\sum_{i=1}^{N} \lambda_i)\Delta t}. \tag{C1}$$

Using the survival function, which is the probability that a random variable exceeds a given value:

$$\int_{\Delta t}^{\infty} \varphi(t')dt' = e^{-(\sum_{i=1}^{N} \lambda_i)\Delta t}, \tag{C2}$$

we have $\Delta t = -\ln u/\sum_{i=1}^{N} \lambda_i$ with $u \in [0, 1]$ uniformly chosen.

(2) *Event determination*. Identify process i that generated the event with probability: $\Pi_i = \lambda_i/\sum_{i=1}^{N} \lambda_i$.

(3) *Process update*. Advance time by Δt and repeat.

b. Laplace Gillespie algorithm

The Laplace Gillespie algorithm is designed for efficient simulation of non-Markovian point processes by utilizing an event-modulated Poisson process; see details in [68]. The key steps are as follows:

(1) Initialize each of the $\mathcal{N}$ processes by drawing the rate s_i $(1 \leqslant i \leqslant \mathcal{N})$ according to its density function $p_i(s_i)$, defined in terms of the WTD $\psi(\tau)$:

$$\psi(\tau) = \int_0^{\infty} p(s) s e^{-s\tau} ds. \tag{C3}$$

Alternatively, integrating both sides one can write

$$\Psi(\tau) = \int_{\tau}^{\infty} \psi(\tau')d\tau' = \int_0^{\infty} p(s) e^{-s\tau} ds. \tag{C4}$$

This entails that $p(s)$ is the inverse Laplace transform of the survival probability $\Psi(\tau)$.

(2) Draw the time until next event $\Delta t = -\ln u/\sum_{j=1}^{\mathcal{N}} s_j$, with $u \in [0, 1]$ uniformly chosen.

(3) Select the process i that has generated the event with probability: $\Pi_i = s_i/\sum_{j=1}^{\mathcal{N}} s_j$.

(4) Draw a new rate s_i according to $p_i(s_i)$. For any process j $(1 \leqslant j \leqslant \mathcal{N})$ whose interevent time statistics have changed following the occurrence of the event in steps 2–3, update their rates λ_j according to modified $p_j(s_j)$.

(5) Repeat steps 2–4 or exit (e.g., upon fixation).

For an exponential distribution (7), we have a Poisson process with rate s_0; i.e., $\psi(\tau) = s_0 e^{-s_0\tau}$ is trivially generated by $p(s) = \delta(s - s_0)$, where δ is the Dirac delta function. For a power-law distribution following Eq. (8), $p(\lambda)$ can be shown to follow a gamma distribution [68] given by

$$p(s) = \frac{s^{\alpha-1} e^{-s/\Lambda_A}}{\Gamma(\alpha)\Lambda_A^{\alpha_A}}, \tag{C5}$$

where $\Gamma(\alpha)$ is the gamma function, α is the shape parameter, and Λ_A is the scale parameter. Similarly, for a gamma WTD

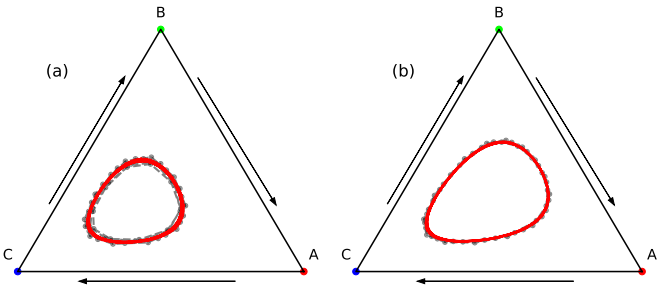

FIG. 6. Dynamics in the ternary simplex for the model of zRPS with the last two reactions of (1) having exponential WTDs with $k_B = k_C = 1$, while the first reaction has a power-law WTD with $(k_A, \alpha_A) = (1, 2)$ in (a), and a gamma WTD with $(k_A, \alpha_A) = (0.4, 0.4)$ in (b). Gray dotted lines are stochastic trajectories $(n_A, n_B, n_C)/N$, averaged over 10^4 realizations starting from the same initial condition (clockwise dynamics), where trajectories are shown for $0 < t \leqslant 100$ (omitting initial transients). Red thick lines: numerical solution of the deterministic rate equations. Corners correspond to the fixation of the labeled species. Here the initial concentrations of A and B are $1/6$ while that of C is $2/3$.

with $\alpha < 1$, $p(s)$ is given by

$$p(s) = \begin{cases} 0, & s < \Lambda_A, \\ [\Gamma(\alpha)\Gamma(1-\alpha)s(s/\Lambda_A - 1)^{\alpha}]^{-1}, & s > \Lambda_A. \end{cases} \tag{C6}$$

Equations (C5) and (C6) are used here to simulate the model with power-law and gamma WTD, respectively.

Importantly, for the gamma WTD $p(s)$ can be used to express the inverse Laplace transform of $\Psi(\tau)$ only for $0 < \alpha < 1$ [68]. Thus, this algorithm cannot be used for gamma WTD with $\alpha > 1$, a regime that will be considered elsewhere with different computational techniques. It is worth noting that, since here $\mathrm{CV}_A(\tau) = \alpha_A^{-1/2}$, it is precisely in the regime where $\alpha_A < 1$ where the WTD is wider than an exponential interevent distribution, which is the main focus of this study.

2. Numerical methods

Here we explain the analysis used to generate Figs. 1 and 3. The deterministic orbits plotted in Fig. 1 (red solid lines) are obtained by numerically solving rate equations (11) for both power-law and gamma WTDs. In the exponential case [Fig. 1(a)] we plot the outermost orbit defined by $\mathcal{R}(t) = 1/N$, where $\mathcal{R}$ is given by (4). For the nonexponential WTD [Figs. 1(b)–1(c)], $\mathcal{R}(t)$ is not necessarily constant and the outermost orbit may not admit a closed form expression. We show the differences between the exponential and nonexponential cases by solving Eqs. (11) with an identical initial condition $\mathcal{R}(t = 0) = 1/N$, which resides on the outermost orbit of the exponential case in Fig. 1(a). The conserved quantity in this figure, $\mathcal{R}(t) = abc^{0.8} = 1/100$, is no longer conserved as can be seen from the clear differences between the red solid lines in Figs. 1(a) and 1(b)–1(c).

In Fig. 3 we compare the theoretical fixed point to the fixed points of the stochastic simulations. To obtain the latter we performed 10^4 realizations with $N = 10^5$, for times $t = 10^3 \ll N$, such that nearly no realization reaches fixation. The steady-state concentrations of A, B, and C in the stochastic dynamics are obtained by averaging each population over all data points in all realizations. Notably, by averaging over all realizations at constant time intervals it is also possible to obtain the dynamic orbits from the stochastic simulations. A typical example of the orbits surrounding the coexistence equilibrium (a^*, b^*, c^*) in the ternary simplex is reported in Fig. 6 for the power-law and gamma WTDs with typical parameters considered in this work. Here all realizations have the same initial concentration of species. In this figure we find good agreement between the averaged stochastic trajectories and numerical solutions of the deterministic rate equation for both classes of WTDs. Finally, in Fig. 7 we show simulation results with a power-law WTD (8) of the concentrations versus time. In Fig. 7(a) we show a single realization, while in Figs. 7(b)–7(c) we show ensemble averages. As expected, the relative fluctuations about the MF equilibrium point (11) decrease as we increase the number of realizations over which the concentrations are averaged.

APPENDIX D: EQUILIBRIUM FOR NONEXPONENTIAL WTDS

Here we obtain the equilibrium point in the general case of arbitrary k_A, k_B, and k_C. Assuming a power-law WTD for the first reaction of (1) and using memory kernel (13) valid for $\alpha_A \gg 1$, the equilibrium of (11) reads

$$\{a^*, b^*, c^*\} = \frac{\{(\alpha_A - 1)k_B, (\alpha_A - 1)k_C, (\alpha_A - 1/2)k_A\}}{(\alpha_A - 1/2)k_A + (\alpha_A - 1)(k_B + k_C)}. \tag{D1}$$

Stability analysis shows that this fixed point remains a nonlinear center in the limit of $\alpha_A \gg 1$; see Appendix A.

In the case of the gamma WTD, one can also compute the equilibrium point in the general case for any α_A. Together with the relation $c^* = 1 - a^* - b^*$, we can solve the rate equations [Eqs. (11)] for arbitrary α_A, finding

$$\{a^*, b^*, c^*\} = \frac{\{2k_B, 2k_C, k_A\alpha_A(3^{1/\alpha_A} - 1)\}}{2(k_B + k_C) + k_A\alpha_A(3^{1/\alpha_A} - 1)}. \tag{D2}$$

The limit $\alpha_A \to 1$ yields $(a^*, b^*, c^*) = (k_B, k_C, k_A)/(k_A + k_B + k_C)$. In contrast, for $\alpha_A \gg 1$, $a^* \simeq k_B/[k_B + k_C + (k_A/2)\ln 3]$, $b^* \simeq k_C/(k_B + k_C + (k_A/2)\ln 3)$, and $c^* \simeq (k_A/2)\ln 3/(k_B + k_C + (k_A/2)\ln 3)$, yielding $a^* = b^* > c^*$ when $k_A = k_B = k_C$. Another important limit is $\alpha_A \to 0$. To leading order in $\alpha_A \ll 1$, the coexistence equilibrium becomes $a^* \simeq 2k_B/(k_A\alpha_A)\,3^{-1/\alpha_A}$, $b^* = (k_C/k_B)a^*$, and $c^* \simeq 1 - 2(k_B + k_C)/(k_A\alpha_A)\,3^{-1/\alpha_A}$. Thus a^* and b^* are exponentially small, whereas c^* asymptotically approaches 1.

Finally, we consider more carefully the limit of $\alpha_A \to 1$. For this, we introduce $\epsilon \equiv \alpha_A - 1$. Assuming that $|\epsilon| \ll 1$, to linear order in ϵ the memory kernel [Eq. (19)] becomes

$$\Theta_G(a, b, c) \simeq 1 - [(3/2)\ln 3 - 1]\varepsilon. \tag{D3}$$

Here the coexistence equilibrium, (D2), becomes

$$a^* = \frac{k_B}{k_A + k_B + k_C}\left[1 + \left(\frac{3\ln 3}{2} - 1\right)\frac{\epsilon k_A}{k_A + k_B + k_C}\right],$$
$$c^* = \frac{k_A}{k_A + k_B + k_C}\left[1 - \left(\frac{3\ln 3}{2} - 1\right)\frac{\epsilon(k_B + k_C)}{k_A + k_B + k_C}\right], \tag{D4}$$

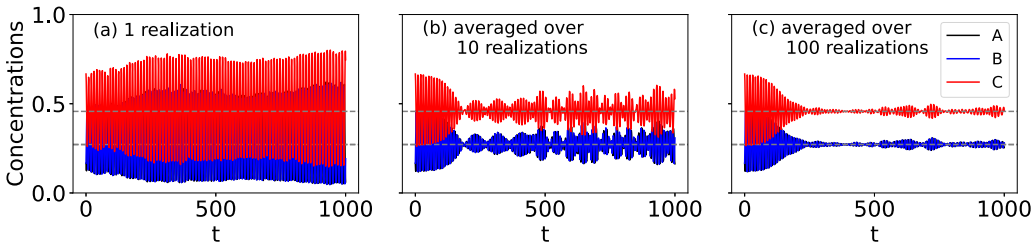

FIG. 7. Shown are concentrations of A (blue), B (black), and C (red) versus time from stochastic simulations for the zRPS model (1) with the last two reactions of (1) having exponential WTDs with $k_B = k_C = 1$, while the first reaction has a power-law WTD with $(k_A, \alpha_A) = (1, 2)$. The solid lines in (a) represent a single realization, while in (b) and (c) they represent ensemble averages over 10 and 100 realizations, respectively. The dashed lines are predictions of Eq. (11). In all panels the total population is $N = 3 \times 10^4$ and the initial concentrations of A and B are $1/6$ while that of C is $2/3$; also note that the concentrations of A and B are overlapping.

with $b^* = (k_C/k_B)a^*$. One can see that for a gamma WTD, changing α_A to be below 1, namely, $\varepsilon < 0$, has the same qualitative effect as having a power-law WTD with finite (but large) α_A. Note that, to obtain Eq. (D3), we have plugged the leading-order in ε of the equilibrium point [Eq. (D4)] into the subleading-order term in ϵ of Θ_G.

In the special case of $k_A = k$ and $k_B = k_C = 1$, Eq. (D4) drastically simplifies, and we can find $k^* = k(\alpha_A)$ for which $a^* = b^* = c^*$: $k^*(\alpha_A) = 1 + [(3/2)\ln 3 - 1](\alpha_A - 1)$ [see Eq. (21)]. The linear nature of the interface between the red and blue phases can be seen in Figs. 4(d)–4(e) close to $\alpha_A = 1$.

[1] K. Tainaka, Paradoxical effect in a three-candidate voter model, Phys. Lett. A **176**, 303 (1993).

[2] M. Frean and E. R. Abraham, Rock-scissors-paper and the survival of the weakest, Proc. R. Soc. London B **268**, 1323 (2001).

[3] B. Kerr, M. Riley, M. Feldman, and B. J. M. Bohannan, Local dispersal promotes biodiversity in a real-life game of rock–paper–scissors, Nature (London) **418**, 171 (2002).

[4] M. Ifti and B. Bergersen, Survival and extinction in cyclic and neutral three-species systems, Eur. Phys. J. E **10**, 241 (2003).

[5] M. Assaf and B. Meerson, Spectral theory of metastability and extinction in birth-death systems, Phys. Rev. Lett. **97**, 200602 (2006).

[6] T. Reichenbach, M. Mobilia, and E. Frey, Coexistence versus extinction in the stochastic cyclic Lotka-Volterra model, Phys. Rev. E **74**, 051907 (2006).

[7] T. Reichenbach, M. Mobilia, and E. Frey, Mobility promotes and jeopardizes biodiversity in rock–paper–scissors games, Nature (London) **448**, 1046 (2007).

[8] G. Szabó and G. Fáth, Evolutionary games on graphs, Phys. Rep. **446**, 97 (2007).

[9] M. Assaf and B. Meerson, Extinction of metastable stochastic populations, Phys. Rev. E **81**, 021116 (2010).

[10] M. Assaf and M. Mobilia, Large fluctuations and fixation in evolutionary games, J. Stat. Mech. (2010) P09009.

[11] A. Müller and J. A. C. Gallas, How community size affects survival chances in cyclic competition games that microorganisms play, Europhys. Lett. **82**, 052901 (2010).

[12] A. Szolnoki, M. Mobilia, L. L. Jiang, B. Szczesny, A. M. Rucklidge, and M. Perc, Cyclic dominance in evolutionary games: A review, J. R. Soc. Interface **11**, 20140735 (2014).

[13] M. Assaf and B. Meerson, WKB theory of large deviations in stochastic populations, J. Phys. A: Math. Theor. **50**, 263001 (2017).

[14] U. Dobramysl, M. Mobilia, M. Pleimling, and U. C. Täuber, Stochastic population dynamics in spatially extended predator–prey systems, J. Phys. A: Math. Theor. **51**, 063001 (2018).

[15] R. West, M. Mobilia, and A. M. Rucklidge, Survival behavior in the cyclic Lotka-Volterra model with a randomly switching reaction rate, Phys. Rev. E **97**, 022406 (2018).

[16] R. West and M. Mobilia, Fixation properties of rock-paper-scissors games in fluctuating populations, J. Theor. Biol. **491**, 110135 (2020).

[17] M. J. Liao, A. Miano, C. B. Nguyen, L. Chao, and J. Hasty, Survival of the weakest in non-transitive asymmetric interactions among strains of *E. coli*, Nat. Commun. **11**, 6055 (2020).

[18] L. Giuggioli and S. Sarvaharman, Spatio-temporal dynamics of random transmission events: From information sharing to epidemic spread, J. Phys. A: Math. Theor. **55**, 375005 (2022).

[19] B. Sinervo and C. M. Lively, The rock-paper-scissors game and the evolution of alternative male strategies, Nature (London) **380**, 240 (1996).

[20] L. Frachebourg, P. L. Krapivsky, and E. Ben-Naim, Spatial organization in cyclic Lotka-Volterra systems, Phys. Rev. E **54**, 6186 (1996).

[21] J. Hofbauer and K. Sigmund, *Evolutionary Games and Population Dynamics* (Cambridge University Press, Cambridge, 1998).

[22] L. Frachebourg and P. Krapivsky, Fixation in a cyclic Lotka-Volterra model, J. Phys. A: Math. Gen. **31**, L287 (1998).

[23] M. Nowak, *Evolutionary Dynamics* (Belknap Press, Cambridge, MA, 2006).

[24] M. Perc, A. Szolnoki, and G. Szabó, Cyclical interactions with alliance-specific heterogeneous invasion rates, Phys. Rev. E **75**, 052102 (2007).

[25] M. Peltomäki and M. Alava, Three- and four-state rock-paper-scissors games with diffusion, Phys. Rev. E **78**, 031906 (2008).

[26] J. C. Claussen and A. Traulsen, Cyclic dominance and biodiversity in well-mixed populations, Phys. Rev. Lett. **100**, 058104 (2008).

[27] M. Mobilia, Oscillatory dynamics in rock-paper-scissors games with mutations, J. Theor. Biol. **264**, 1 (2010).

[28] L.-L. Jiang, T. Zhou, M. Perc, and B.-H. Wang, Effects of competition on pattern formation in the rock-paper-scissors game, Phys. Rev. E **84**, 021912 (2011).

[29] Q. He, M. Mobilia, and U. C. Täuber, Spatial rock-paper-scissors models with inhomogeneous reaction rates, Phys. Rev. E **82**, 051909 (2010).
[30] Q. He, M. Mobilia, and U. Täuber, Coexistence in the two-dimensional May-Leonard model with random rates, Eur. Phys. J. B **82**, 97 (2011).
[31] B. Szczesny, M. Mobilia, and A. M. Rucklidge, When does cyclic dominance lead to spiral waves? Europhys. Lett. **102**, 28012 (2013).
[32] B. Szczesny, M. Mobilia, and A. M. Rucklidge, Characterization of spiraling patterns in spatial rock-paper-scissors games, Phys. Rev. E **90**, 032704 (2014).
[33] E. Kelsic, J. Zhao, K. Vetsigian, and R. Kishony, Counteraction of antibiotic production and degradation stabilizes microbial communities, Nature (London) **521**, 516 (2015).
[34] D. F. P. Toupo and S. H. Strogatz, Nonlinear dynamics of the rock-paper-scissors game with mutations, Phys. Rev. E **91**, 052907 (2015).
[35] M. Mobilia, A. M. Rucklidge, and B. Szczesny, The influence of mobility rate on spiral waves in spatial rock-paper-scissors games, Games **7**, 24 (2016).
[36] C. M. Postlethwaite and A. M. Rucklidge, Spirals and heteroclinic cycles in a spatially extended rock-paper-scissors model of cyclic dominance, Europhys. Lett. **117**, 48006 (2017).
[37] B. L. Brown, H. Meyer-Ortmanns, and M. M. Pleimling, Dynamically generated hierarchies in games of competition, Phys. Rev. E **99**, 062116 (2019).
[38] R. Baker and M. M. Pleimling, The effect of habitats and fitness on species coexistence in systems with cyclic dominance, J. Theor. Biol. **486**, 110084 (2020).
[39] S. Islam, A. Mondal, M. Mobilia, S. Bhattacharyya, and C. Hens, Effect of mobility in the rock-paper-scissor dynamics with high mortality, Phys. Rev. E **105**, 014215 (2022).
[40] M. Berr, T. Reichenbach, M. Schottenloher, and E. Frey, Zero-one survival behavior of cyclically competing species, Phys. Rev. Lett. **102**, 048102 (2009).
[41] L. J. S. Allen, *An Introduction to Stochastic Processes with Applications to Biology* (CRC Press, Boca Raton, FL, 2010).
[42] G. M. Viswanathan, S. V. Buldyrev, S. Havlin, M. G. da Luz, E. P. Raposo, and H. E. Stanley, Optimizing the success of random searches, Nature (London) **401**, 911 (1999).
[43] R. Metzler, J.-H. Jeon, G. H. Cherstvy, and E. Barkai, Anomalous diffusion models and their properties: Non-stationarity, non-ergodicity, and ageing at the centenary of single particle tracking, Phys. Chem. Chem. Phys. **16**, 24128 (2014).
[44] M. E. Wosniack, M. C. Santos, E. P. Raposo, G. M. Viswanathan, and M. G. da Luz, The evolutionary origins of Lévy walk foraging, PLoS Comput. Biol. **13**, e1005774 (2017).
[45] B. Guinard and A. Korman, Intermittent inverse-square Lévy walks are optimal for finding targets of all sizes, Sci. Adv. **7**, eabe8211 (2021).
[46] O. Vilk, Y. Orchan, M. Charter, N. Ganot, S. Toledo, R. Nathan, and M. Assaf, Ergodicity breaking in area-restricted search of avian predators, Phys. Rev. X **12**, 031005 (2022).
[47] F. Jafarpour, E. Levien, and A. Amir, Evolutionary dynamics in non-Markovian models of microbial populations, Phys. Rev. E **108**, 034402 (2023).
[48] C. C. Costa, G. Sridhar, C. Wyart, and M. Vergassola, Fluctuating landscapes and heavy tails in animal behavior, PRX Life **2**, 023001 (2024).
[49] M. Giannakou and B. Waclaw, Resonant noise amplification in a predator-prey model with quasi-discrete generations, Sci. Rep. **14**, 16783 (2024).
[50] O. Vilk, E. Aghion, T. Avgar, C. Beta, O. Nagel, A. Sabri, R. Sarfati, D. K. Schwartz, M. Weiss, D. Krapf *et al.*, Unravelling the origins of anomalous diffusion: From molecules to migrating storks, Phys. Rev. Res. **4**, 033055 (2022).
[51] O. Vilk, D. Campos, V. Méndez, E. Lourie, R. Nathan, and M. Assaf, Phase transition in a non-Markovian animal exploration model with preferential returns, Phys. Rev. Lett. **128**, 148301 (2022).
[52] O. Vilk, E. Aghion, R. Nathan, S. Toledo, R. Metzler, and M. Assaf, Classification of anomalous diffusion in animal movement data using power spectral analysis, J. Phys. A: Math. Theor. **55**, 334004 (2022).
[53] C. W. Gardiner, *Handbook of Stochastic Methods* (Springer, New York, 2002).
[54] N. van Kampen, *Stochastic Processes in Physics and Chemistry* (North-Holland, Amsterdam, 1992).
[55] M. Broom and J. Rychtář, *Game-Theoretical Models in Biology* (CRC Press, Boca Raton, FL, 2013).
[56] When the initial number of individuals of each species is identical, the law of stay out predicts that the species that is "least engaged" in interactions is the most likely to survive/fixate [15,16,40].
[57] Alternatively, one can demand that the WTD's *median*, $\bar{\tau}_{\mathrm{A}}$ be equal that of the exponential distribution. This enables comparing, e.g., WTDs that have a diverging mean.
[58] T. Aquino and M. Dentz, Chemical continuous time random walks, Phys. Rev. Lett. **119**, 230601 (2017).
[59] O. Vilk, R. Metzler, and M. Assaf, Non-Markovian gene expression, Phys. Rev. Res. **6**, L022026 (2024).
[60] This approximation holds, since the integrand is maximal at $\ell = 1$, and when $m, z \gg 1$, one can Taylor expand the integrand around $\ell = 1$.
[61] A. Amir, Cell size regulation in bacteria, Phys. Rev. Lett. **112**, 208102 (2014).
[62] T. Nozoe and E. Kussell, Cell cycle heritability and localization phase transition in growing populations, Phys. Rev. Lett. **125**, 268103 (2020).
[63] A. Szolnoki and M. Perc, Biodiversity in models of cyclic dominance is preserved by heterogeneity in site-specific invasion rates, Sci. Rep. **6**, 38608 (2016).
[64] P. Avelino, D. Bazeia, L. Losano, J. Menezes, and B. de Oliveira, Spatial patterns and biodiversity in off-lattice simulations of a cyclic three-species Lotka-Volterra model, Europhys. Lett. **121**, 48003 (2018).
[65] O. Vilk, M. Mobilia, and M. Assaf, Supporting data and codes, GitLab (2025), https://gitlab.com/ohad.vilk/non_exponential_rock_paper_scissors.
[66] O. Vilk and M. Assaf, Escape from a metastable state in non-Markovian population dynamics, Phys. Rev. E **110**, 044132 (2024).
[67] D. Gillespie, A general method for numerically simulating the stochastic time evolution of coupled chemical reactions, J. Comput. Phys. **22**, 403 (1976).
[68] N. Masuda and L. E. Rocha, A Gillespie algorithm for non-Markovian stochastic processes, SIAM Rev. **60**, 95 (2018).